Letter

Synthesis and Structural Characterization of Branched Bimetallic AuPd Nanoparticles with a Highly Tunable Optical Response

Silvia Nuti, Adrián Fernández-Lodeiro,* Lidia E. Chinchilla, Ana B. Hungría, José-Luis Capelo-Martinez, Carlos Lodeiro, and Javier Fernández-Lodeiro*

Read Online

ACCESS | Metrics & More | Article Recommendations | Supporting Information

ABSTRACT: Bimetallic nanostructures composed of gold (Au) and palladium (Pd) have garnered increased interest for their applications in heterogeneous catalysis. This study reports a simple strategy for manufacturing Au@Pd bimetallic branched nanoparticles (NPs), which offer a tunable optical response, using polyallylamine-stabilized branched AuNPs as template cores for Pd overgrowth. The palladium content can be altered by manipulating the concentration of $PdCl_4^{2-}$ and ascorbic acid (AA) that are injected, which permit an overgrowth of the Pd shell up to ca. 2 nm thick. The homogeneous distribution of Pd at the surfaces of Au NPs can be carried out regardless of their size or branching degree, which allows for an adjustment of the plasmon response in the near-infrared (NIR) spectral range. As a proof of concept, the nanoenzymatic activity of pure gold and gold–palladium NPs was compared, exploring their peroxidase-like activity in the oxidation of 3,3′,5,5′-tetramethyl-benzidine (TMB). The bimetallic AuPd NPs demonstrate an increase in the catalytic properties attributed to the presence of palladium at the surface of gold.
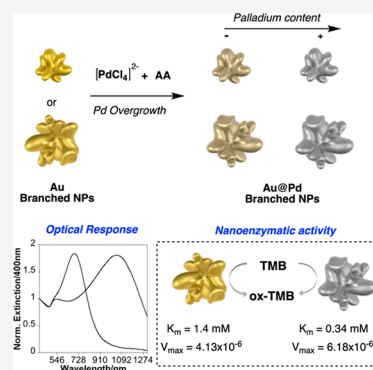
Bimetallic nanoparticles (NPs), which consist of a core@shell or alloy structure, have been the subject of extensive research over the last decades. These particles possess unique physical and chemical properties that can be harnessed through synergistic effects between different metals.[1,2] For example, because palladium (Pd) has weak plasmonic properties, combining it with gold (Au) to produce core@shell or alloy AuPd NPs has sparked intensive research aimed at exploiting the superior catalytic properties of Pd in combination with the excellent optical properties of gold.[3,4]

Following successful control in synthesizing spherical AuPd NPs that exhibit improved or novel properties,[5−7] researchers have turned their attention to developing anisotropic AuPd NPs. These particles can take advantage of the shape-dependent optical response of Au while allowing for control of the exposed crystallographic facets, which is crucial for catalytic properties.[8]

For example, gold nanorods, nanocubes, and nanoplates have been used as templates to create a variety of bimetallic nanostructures that have shown promise in catalysis[9,10] or biochemical sensing,[11] among others.

Considering that the branched Au NPs offer an intense and tunable plasmon response in the visible–near-infrared (vis–NIR) region with intense scattered electromagnetic fields located at the tips,[12] these particular gold NPs should be considered exciting candidates for manufacturing plasmonic active core@shell or alloy AuPd bimetallic NPs with potential photothermal,[13] catalytic,[14] or surface-enhanced Raman scattering (SERS) substrate[15] applications.

Although one-step syntheses of branched AuPd NPs have been developed, they usually yield bimetallic NPs with limited size control[15] and/or optical response.[16,17] In contrast, seed-mediated strategies have emerged as a promising alternative as a result of their ability to provide precise control over the size, morphology, and composition of the particles, leading to enhanced control over their properties.[13]

Branched bimetallic NPs have mainly been synthesized through seeded co-reduction processes in surfactant solutions. This approach, first demonstrated by DeSantis and colleagues,[18] has resulted in the successful synthesis of octopods or concave AuPd nanocrystals with flexible plasmon tuning capabilities that depend upon their morphology and composition.[19] In other seed-mediated co-reduction processes, utilizing polyvinylpyrrolidone (PVP) as a stabilizer and $AgNO_3$ as a shape director, AuPd nanostars with high[20] or low[21] palladium content were synthesized. These nanostars have shown excellent catalytic performance, although with limited localized surface plasmon resonance (LSPR) band tunability.

In contrast, template strategies using branched gold NPs as seeds are limited, partly because these nanostructures are prone to reshaping; weakly bonded atoms at the tips tend to
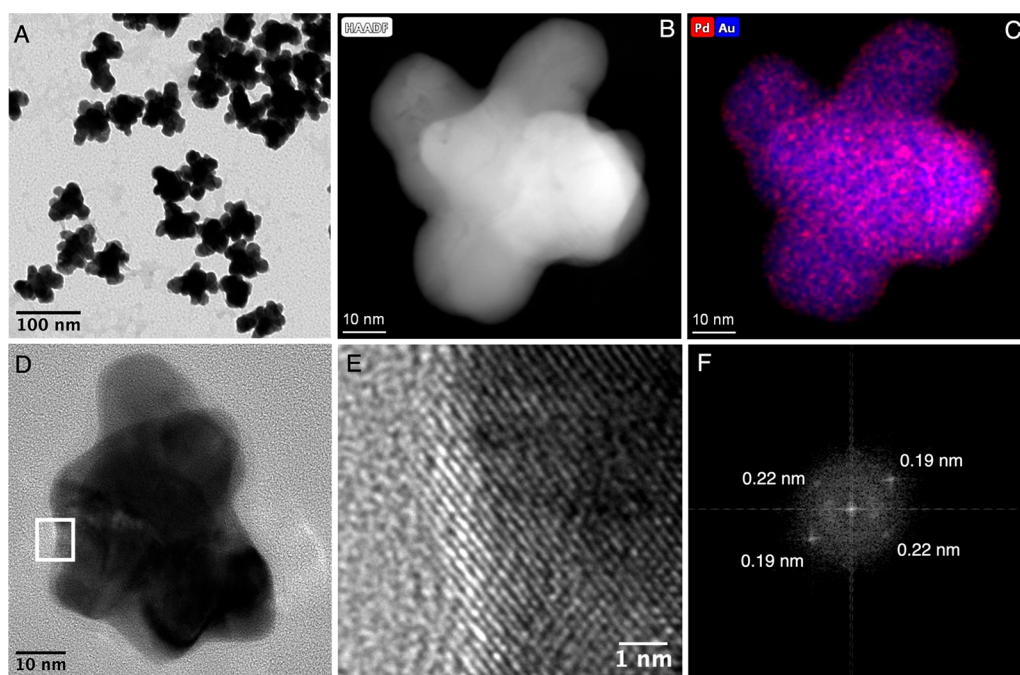
Figure 1. (A) Low-magnification TEM image showing typical NP morphology of branched AuPd NPs obtained with a molar ratio Au:Pd of 1:0.1. (B) High-magnification HAADF-STEM image of individual AuPd particles together with the (C) Au and Pd distribution XEDS maps of the same NP. The outer area marked with a white box in the particle shown in panel D exhibits high-resolution contrasts in panel E, and the crystal spacings are measured in the DDP shown in panel F.

migrate to more stable regions, resulting in increased sphericity, thus affecting their optical response.[21] Recently, gold multipod NPs were used in a template synthesis to achieve epitaxial or island growth of Pd. The resulting bimetallic NPs exhibited a substantially enhanced electrochemical oxygen reduction reaction (ORR) activity compared to their gold counterparts, although with limited optical response.[14] Consequently, there is a strong demand for novel synthesis pathways that enable the deposition of palladium onto branched gold NPs with plasmonic activity.

In the present work, we devised a simple template methodology, assisted by poly(allylamine hydrochloride) (PAH), to obtain AuPd branched NPs in an aqueous phase and at room temperature, with a tunable optical response. In a typical synthesis, polyallylamine was used to assist the synthesis of polycrystalline branched gold NPs through kinetically controlled growth on small multi-twinned gold seeds. By adjustment of the pH and/or seed concentration, the sizes and branched morphology could be finely tuned, resulting in a plasmon response that ranged from red to infrared wavelengths (560−1250 nm).[22]

The surface of the branched NPs presents numerous exposed amine groups originating from the polyallylamine chains. Given the affinity of $PdCl_2$ toward polyallylamine,[23] the formation of an adequate substrate is expected for the interaction with Pd(II), assisting their reduction at the gold surface.

In a typical synthesis to obtain AuPd NPs, gold branched NPs are first synthesized. Then, in the same vessel, K_2PdCl_4 and, subsequently, ascorbic acid (AA) are injected (see the Experimental Section of the Supporting Information for details). The bimetallic NPs synthesized with Au:Pd molar ratio of 1:0.1 retained the branched morphology as their Au monometallic counterpart (Figure 1A) without appreciable changes in the overall dimension, maintaining a very

homogeneous particle size distribution (Figure S1 of the Supporting Information). The high-angle annular dark-field scanning transmission electron microscopy (HAADF-STEM) images, together with the X-ray energy-dispersive spectroscopy (XEDS) compositional maps acquired in STEM mode, show that palladium is distributed throughout the surface of the NPs, with no surface enrichment of palladium detected (panels B and C of Figure 1 and Figure S2 of the Supporting Information). The Au:Pd atomic ratio in the NPs, calculated from the quantification of the XEDS spectra acquired at each pixel of the images, as shown in Figure 1C, indicated a 4.8 atomic % of Pd-balanced Au for a large number of analyzed NPs (Figure S2 of the Supporting Information).

High-resolution transmission electron microscopy (HRTEM) images reveal the crystalline structure of the tips of the NPs (the thinnest regions) (panels D and E of Figure 1 and Figure S3 of the Supporting Information). When a fast Fourier transform (FFT) is performed on the HRTEM image, distances of 0.22 and 0.19 nm can be measured in the digital diffraction pattern (DDP) (Figure 1F and Figures S3−S5 of the Supporting Information), which should correspond to the {111} and {200} planes, respectively, of the face-centered cubic (fcc) structure of palladium.[24,25] However, a continuous metal shell surrounding the particles was not observed. Therefore, according to HAADF-STEM and HRTEM images, it seems that palladium is localized in discrete regions that exhibit uniform dispersion throughout the entirety of the NP surface rather than forming a very thin uniform layer.

It is interesting to note that, by increasing the concentration of $PdCl_4^{2-}$ and AA, there is a transition from a situation in which gold and palladium are homogeneously distributed on the surface of the NPs to a well-defined core@shell structure. When the Au:Pd molar ratio is increased to 1:1, the NPs exhibit a regular palladium shell with an average thicknesses ranging between ~1.5 and 2 nm, as revealed in high-resolution
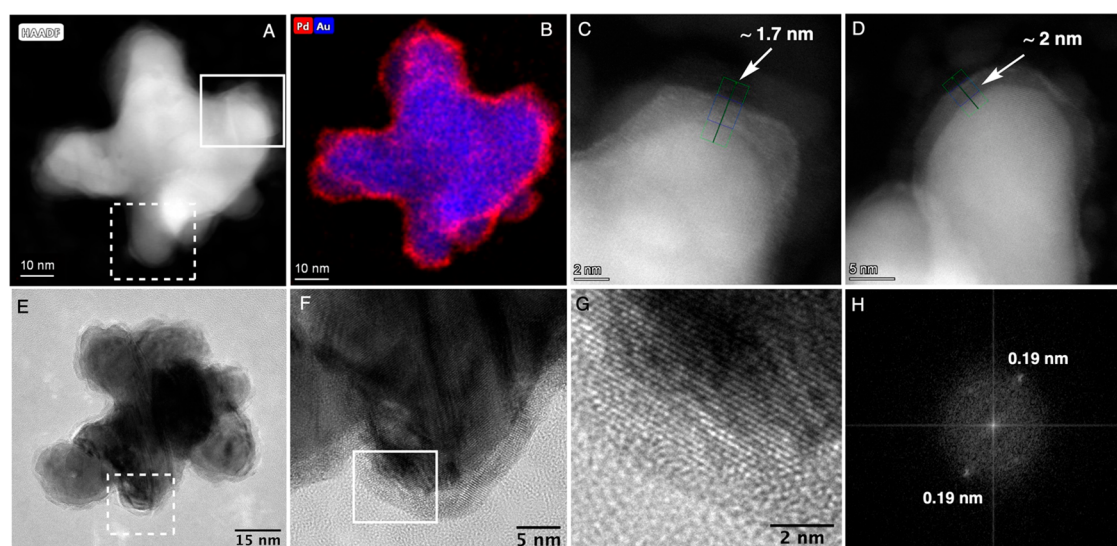
Figure 2. (A) HAADF-STEM image and (B) XEDS map of a NP obtained with Au:Pd molar ratio of 1:1 showing the distribution of gold and palladium. (C and D) High-magnification HAADF images where Pd shells can be measured. (E−G) TEM images were obtained at increasing magnification of one NP. The dashed white box in panel E is magnified in panel F, and the solid white box in panel F corresponds to the area shown in panel G. Finally, panel H shows the DDP of the area displayed in panel G.
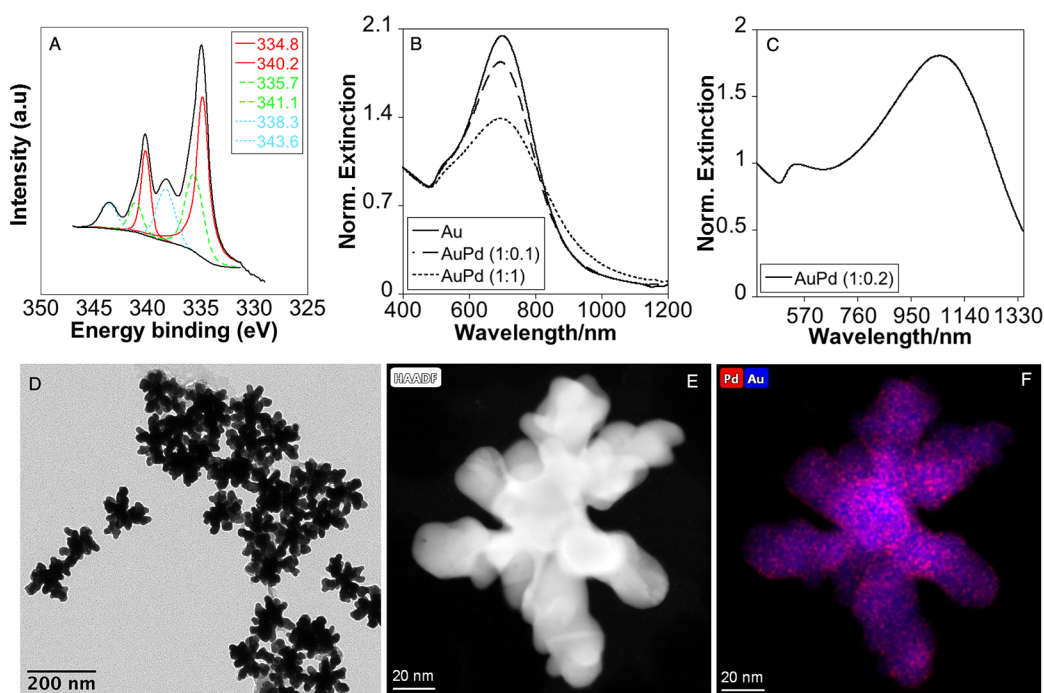

Figure 3. (A) XPS spectra of AuPd NPs. (B) Normalized extinction spectra of Au and AuPd NPs produced using 53.3 pM gold seeds and different Au:Pd molar ratios. (C) Normalized extinction spectra of AuPd NPs were obtained using 13.3 pM gold seeds and the Au:Pd molar ratio of 1:0.2. (D) Low-magnification TEM image showing typical NP morphology of branched AuPd NPs using 13.3 pM gold seeds and under the Au:Pd molar ratio of 1:0.2. (E) HAADF-STEM images together with the (F) XEDS map of a NP showing Au and Pd distribution.

HAADF-STEM (panels A−D of Figure 2) and HRTEM images (panels E−G of Figure 2). The quantitative composition of several AuPd NPs determined from XEDS spectrum image maps shows an increase in the average Pd content with respect to the NPs obtained at a molar ratio 1:0.1 reaching 20.8 atomic % of Pd-balanced Au for many analyzed NPs (Figure S6 of the Supporting Information). High-resolution images of the tips showed the presence of a shell with a lower contrast when compared to the gold core, which presented clear lattice fringes, indicating the successful

deposition of a metallic Pd shell on the surface of gold (panels E−G of Figure 2 and Figure S7 of the Supporting Information). FFT on the HRTEM image obtained from the tips showed a DDP with abundant spots at d spacing of 0.19 nm (Figure 1F) and 0.22 nm (Figures S7 and S8 of the Supporting Information), which should correspond to {111} and {200} fcc Pd structures, respectively.[24,25]

X-ray photoelectron spectroscopy (XPS) of the branched NPs shows the typical doublets for the Au 4f XPS, at 83.9 and 87.5 eV originated from the gold body (see Figure S9 of the

Supporting Information).[26] The XPS in the Pd region obtained for AuPd (1:1) shows that the signals from the Pd 3d region display three doublets (see Figure 3A). The peaks at 334.8 and 340.2 eV and the peaks at 338.3 and 343.6 eV can be attributed to Pd[0] and Pd[2+], respectively.[27,28] Furthermore, signals at 335.7 and 341.1 eV can also be ascribed to zero-valent Pd.[29] This can be related with an initial formation of the AuPd alloy, represented by peaks at 334.8 and 340.2 eV, while the metallic Pd shell is represented with the peaks at 335.7 and 341.1 eV, which correspond to the double peaks observed in monometallic Pd NPs.[30]

The optical response of bimetallic NPs shows a damping of the main LSPR, consistent with the Pd content at the surfaces (Figure S10 of the Supporting Information). Where a slight damping is observed for Au:Pd (1:0.1), a more pronounced damping with a broader LSPR response is obtained for AuPd (1:1) (Figure 3B). Notably, although there is a marked blue shift of the main LSPR just after Pd(II)/AA injection, a further red shift is observed, stabilizing the LSPR band after 24 h (see Figure S10 of the Supporting Information) and bringing it close to its Au counterpart. This behavior could be associated with the reduction/oxidation processes of Pd and/or Au on the surfaces of the gold branches, which can undergo reshaping during the formation of bimetallic NPs, thus altering their optical response. Importantly, even with a relatively homogeneous shell thickness of about 2 nm, the LSPR band remains discernible, as previously observed in gold nanorods coated with Pd.[31]

Gold NPs with a highly branched morphology and a LSPR band over 1000 nm were utilized as a template to further investigate plasmon tunability. These NPs were synthesized by reducing the concentration of the initial gold seeds to 13.3 pM. During the deposition process, we observed a lower palladium deposition under the same conditions. To obtain a comparable amount of palladium on the surface of the more branched NPs, a molar ratio of Au:Pd of 1:0.2 was necessary. The obtained branched NPs obtained showed an intense and defined LSPR band with λ_{max} over 1000 nm (Figure 3C). The TEM images of the NPs synthesized under these conditions show a hyperbranched morphology with a homogeneous palladium distribution on the surface, as indicated in the XEDS maps obtained from HAADF-STEM images (panels D−F of Figure 3). The quantitative analysis of the XEDS maps of several particles reveals a 4.9 atomic % of Pd-balanced Au (Figure S11 of the Supporting Information). When the Au:Pd molar ratio was increased to 1:1, the high-magnification XEDS maps revealed an increase in the Pd content on the surface (see Figure S12 of the Supporting Information). The HRTEM images showed that the NPs had a surface enriched with {111} and {200} fcc Pd crystal structures, which were indicated by the spots at d spacings of 0.19 and 0.22 nm in the DDP (Figure S13 of the Supporting Information). However, unlike their smaller counterparts produced at the same AuPd ratio (Figure 2), a separate Pd metallic shell was not clearly observed in the images (Figure S12 of the Supporting Information).

With regard to colloidal stability, AuPd branched NPs remain stable in water for at least 2 weeks after purification, showing a ζ potential of +21.6 mV (see Figure S14 of the Supporting Information). However, storing the NPs for longer periods of time leads to a decrease in their ζ potential, as shown in Figure S15A of the Supporting Information. This decrease in the ζ potential is associated with a decline in their colloidal stability, ultimately resulting in their aggregation, as observed in dynamic light scattering (DLS) studies (Figure S15B of the Supporting Information). Interestingly, when the NPs are extra-functionalized with PAH, they retain their colloidal properties for a minimum duration of 2 months at room temperature, demonstrating stability over an extended period (panels C and D of Figure S15 of the Supporting Information).

Finally, it should be mentioned that, although high control in the morphology and branching of optically active AuPd NPs has been achieved in the past, they are usually obtained in surfactants, such as cetyltrimethylammonium bromide (CTAB) and cetyltrimethylammonium chloride (CTAC),[18,19] which can make their subsequent functionalization difficult. In this regard, the positive surface charge of AuPd NPs originated from the amine groups of polyallylamine chains can offer additional benefits for future materials when it comes to post-functionalization, as demonstrated in the case of pure gold NPs.[22]

To investigate the catalytic activity after palladium coating, we studied the ability of Au and AuPd branched NPs to mimic the peroxidase-like activity of enzymes.[32] We employed tetramethylbenzidine (TMB) as a substrate, which is oxidized to form a blue compound (oxidized TMB) in the presence of hydrogen peroxide. For this study, we selected Au and AuPd (Au:Pd of 1:1) NPs with the main LSPR band over 1000 nm to minimize the coincidence between the LSPR band and the absorption band of the TMB oxidation product.

To determine the peroxidase-like activity, we tested different concentrations of TMB (see the Experimental Section of the Supporting Information). Using the Lineweaver−Burk equation, we calculated the estimated values of the Michaelis−Menten constant (K_m) and the maximum reaction velocity (V_{max}). The Au NPs exhibited K_m and V_{max} values for TMB of 1.4 mM and 4.13×10^{-6} M min^{-1}, respectively. In contrast, the AuPd NPs displayed improved catalytic activity and TMB affinity, with K_m and V_{max} values of 0.34 mM and 6.18×10^{-6} M min^{-1}, respectively (Figure S16 of the Supporting Information). These findings suggest that the simple addition of PdCl$_4^{2-}$ and AA to the gold NPs resulted in superior catalytic properties compared to those of their monometallic counterparts, highlighting the potential of the system for generating high-performance catalytic nanomaterials for peroxidase-like nanozymes.

In conclusion, our study describes the synthesis of bimetallic gold−palladium branched NPs with a flexible optical response. The LSPR band can be finely tuned according to the size and branching morphology of Au NPs selected as the template. For instance, branched AuPd NPs with a mean size of approximately 75 nm and LSPR band in ca. 700 nm can be manufactured with different palladium contents, which allows for the acquisition from a state in which gold and palladium are evenly distributed on the surface of the NPs to a distinct core−shell structure with a thickness of approximately 2 nm simply by adjusting the Au:Pd molar ratio during synthesis.

Furthermore, Pd deposition can be achieved in NPs with a bigger size and branching degree without degrading their LSPR band, resulting in the formation of branched AuPd heterostructures with an optical response above 1000 nm. Notably, these bimetallic NPs showed an improved nano-enzyme activity when compared to their gold counterpart.

Further research should address the achievable thickness limits of the palladium shell over the complete library of branched AuNPs produced with PAH, which would provide

valuable insights and knowledge for designing and fabricating plasmonic heterostructures. Nevertheless, our study presents a straightforward synthetic route that utilizes the affinity of amine residues in PAH toward Pd(II) for manufacturing AuPd NPs. Such structures could maximize the catalytic properties that result from combining Au and Pd and, importantly, open a door for the photocatalytic application, making the findings of this study highly relevant.

ASSOCIATED CONTENT

Supporting Information

The Supporting Information is available free of charge at https://pubs.acs.org/doi/10.1021/acs.jpclett.3c01431.

Experimental details and additional material characterization, including UV−vis, LR-TEM, HR-TEM, HAADF-STEM, EDS, XPS, ζ potential, and DLS (PDF)

AUTHOR INFORMATION

Corresponding Authors

Adrián Fernández-Lodeiro − *BIOSCOPE Research Group, LAQV-REQUIMTE, Chemistry Department, NOVA School of Science and Technology, FCT NOVA, Universidade NOVA de Lisboa, 2829-516 Caparica, Portugal; PROTEOMASS Scientific Society, Rúa dos Inventores, Madan Parque, 2829-516 Caparica, Portugal;* Email: a.lodeiro@fct.unl.pt

Javier Fernández-Lodeiro − *BIOSCOPE Research Group, LAQV-REQUIMTE, Chemistry Department, NOVA School of Science and Technology, FCT NOVA, Universidade NOVA de Lisboa, 2829-516 Caparica, Portugal; PROTEOMASS Scientific Society, Rúa dos Inventores, Madan Parque, 2829-516 Caparica, Portugal;* orcid.org/0000-0001-8853-2631; Email: j.lodeiro@fct.unl.pt

Authors

Silvia Nuti − *BIOSCOPE Research Group, LAQV-REQUIMTE, Chemistry Department, NOVA School of Science and Technology, FCT NOVA, Universidade NOVA de Lisboa, 2829-516 Caparica, Portugal;* orcid.org/0000-0003-1420-6109

Lidia E. Chinchilla − *Departamento de Ciencia de los Materiales e Ingeniería Metalúrgica y Química Inorgánica. Facultad de Ciencias, Universidad de Cádiz, 11510 Puerto Real, Cádiz, Spain;* orcid.org/0000-0002-5936-0807

Ana B. Hungría − *Departamento de Ciencia de los Materiales e Ingeniería Metalúrgica y Química Inorgánica. Facultad de Ciencias, Universidad de Cádiz, 11510 Puerto Real, Cádiz, Spain;* orcid.org/0000-0002-4622-6967

José-Luis Capelo-Martinez − *BIOSCOPE Research Group, LAQV-REQUIMTE, Chemistry Department, NOVA School of Science and Technology, FCT NOVA, Universidade NOVA de Lisboa, 2829-516 Caparica, Portugal; PROTEOMASS Scientific Society, Rúa dos Inventores, Madan Parque, 2829-516 Caparica, Portugal;* orcid.org/0000-0001-6276-8507

Carlos Lodeiro − *BIOSCOPE Research Group, LAQV-REQUIMTE, Chemistry Department, NOVA School of Science and Technology, FCT NOVA, Universidade NOVA de Lisboa, 2829-516 Caparica, Portugal; PROTEOMASS Scientific Society, Rúa dos Inventores, Madan Parque, 2829-516 Caparica, Portugal;* orcid.org/0000-0001-5582-5446

Complete contact information is available at:
https://pubs.acs.org/10.1021/acs.jpclett.3c01431

Notes

The authors declare no competing financial interest.

ACKNOWLEDGMENTS

REFERENCES

(1) Liu, H.; Nosheen, F.; Wang, X. Noble Metal Alloy Complex Nanostructures: Controllable Synthesis and Their Electrochemical Property. *Chem. Soc. Rev.* **2015**, *44* (10), 3056−3078.

(2) Zhang, M.; Guo, X. Gold/Platinum Bimetallic Nanomaterials for Immunoassay and Immunosensing. *Coord. Chem. Rev.* **2022**, *465*, No. 214578.

(3) Sytwu, K.; Vadai, M.; Dionne, J. A. Bimetallic Nanostructures: Combining Plasmonic and Catalytic Metals for Photocatalysis. *Adv. Phys. X* **2019**, *4* (1), No. 1619480.

(4) Pramanick, B.; Felix Siril, P. Synergistic Visible Light Plasmonic Photocatalysis of Bi-Metallic Gold-Palladium Nanoparticles Supported on Graphene. *Results Chem.* **2023**, *5*, No. 100774.

(5) Hu, J.-W.; Li, J.-F.; Ren, B.; Wu, D.-Y.; Sun, S.-G.; Tian, Z.-Q. Palladium-Coated Gold Nanoparticles with a Controlled Shell Thickness Used as Surface-Enhanced Raman Scattering Substrate. *J. Phys. Chem. C* **2007**, *111* (3), 1105−1112.

(6) Boltersdorf, J.; Leff, A. C.; Forcherio, G. T.; Baker, D. R. Plasmonic Au−Pd Bimetallic Nanocatalysts for Hot-Carrier-Enhanced Photocatalytic and Electrochemical Ethanol Oxidation. *Crystals* **2021**, *11* (3), 226.

(7) Fernández-Lodeiro, C.; Fernández-Lodeiro, J.; Carbó-Argibay, E.; Lodeiro, C.; Pérez-Juste, J.; Pastoriza-Santos, I. The Versatility of Fe(II) in the Synthesis of Uniform Citrate-Stabilized Plasmonic Nanoparticles with Tunable Size at Room Temperature. *Nano Res.* **2020**, *13* (9), 2351−2355.

(8) Sun, L.; Zhang, Q.; Li, G. G.; Villarreal, E.; Fu, X.; Wang, H. Multifaceted Gold−Palladium Bimetallic Nanorods and Their Geometric, Compositional, and Catalytic Tunabilities. *ACS Nano* **2017**, *11* (3), 3213−3228.

(9) Su, G.; Jiang, H.; Zhu, H.; Lv, J.-J.; Yang, G.; Yan, B.; Zhu, J.-J. Controlled Deposition of Palladium Nanodendrites on the Tips of Gold Nanorods and Their Enhanced Catalytic Activity. *Nanoscale* **2017**, *9* (34), 12494−12502.

(10) Roy, A.; Paital, D.; Khatua, S. Pd-Coated Au Triangular Nanoprisms as Catalysts for Hot-Carrier-Driven Photochemistry. *ACS Appl. Nano Mater.* **2022**, *5* (3), 4437−4446.

(11) Fan, H.; Li, Y.; Liu, J.; Cai, R.; Gao, X.; Zhang, H.; Ji, Y.; Nie, G.; Wu, X. Plasmon-Enhanced Oxidase-Like Activity and Cellular Effect of Pd-Coated Gold Nanorods. *ACS Appl. Mater. Interfaces* **2019**, *11* (49), 45416−45426.

(12) Reguera, J.; Langer, J.; Jiménez De Aberasturi, D.; Liz-Marzán, L. M. Anisotropic Metal Nanoparticles for Surface Enhanced Raman Scattering. *Chem. Soc. Rev.* **2017**, *46* (13), 3866−3885.

(13) Quintanilla, M.; Kuttner, C.; Smith, J. D.; Seifert, A.; Skrabalak, S. E.; Liz-Marzán, L. M. Heat Generation by Branched Au/Pd Nanocrystals: Influence of Morphology and Composition. *Nanoscale* **2019**, *11* (41), 19561−19570.

(14) Duy Mai, H.; Kim, S.; Yoo, H. Controllable Growth of Palladium on Gold Multipod Nanoparticles and Their Enhanced Electrochemical Oxygen Reduction Reaction Performances. *J. Catal.* **2020**, *388*, 20−29.

(15) Feng, J.-J.; Lin, X.-X.; Chen, S.-S.; Huang, H.; Wang, A.-J. Thymine-Directed Synthesis of Highly Branched Gold-Palladium Alloy Nanobrambles as a Highly Active Surface-Enhanced Raman Scattering Substrate. *Sensors Actuators B Chem.* **2017**, *247*, 490−497.

(16) Abdul Hakkeem, H. M.; Babu, A.; Shilpa, N.; Venugopal, A. A.; Mohamed, A. P.; Kurungot, S.; Pillai, S. Tailored Synthesis of Ultra-Stable Au@Pd Nanoflowers with Enhanced Catalytic Properties Using Cellulose Nanocrystals. *Carbohydr. Polym.* **2022**, *292* (June), No. 119723.

(17) Choi, Y. S.; Ji, M.-J.; Kim, Y. J.; Kim, H. J.; Hong, J. W.; Lee, Y. W. One-Pot Au@Pd Dendritic Nanoparticles as Electrocatalysts with Ethanol Oxidation Reaction. *Catalysts* **2023**, *13* (1), 11.

(18) DeSantis, C. J.; Peverly, A. A.; Peters, D. G.; Skrabalak, S. E. Octopods versus Concave Nanocrystals: Control of Morphology by Manipulating the Kinetics of Seeded Growth via Co-Reduction. *Nano Lett.* **2011**, *11* (5), 2164−2168.

(19) DeSantis, C. J.; Skrabalak, S. E. Size-Controlled Synthesis of Au/Pd Octopods with High Refractive Index Sensitivity. *Langmuir* **2012**, *28* (24), 9055−9062.

(20) Ma, T.; Liang, F.; Chen, R.; Liu, S.; Zhang, H. Synthesis of Au-Pd Bimetallic Nanoflowers for Catalytic Reduction of 4-Nitrophenol. *Nanomaterials* **2017**, *7* (9), 239.

(21) Ma, T.; Liang, F. Au−Pd Nanostars with Low Pd Content: Controllable Preparation and Remarkable Performance in Catalysis. *J. Phys. Chem. C* **2020**, *124* (14), 7812−7822.

(22) Nuti, S.; Fernández-Lodeiro, C.; Fernández-Lodeiro, J.; Fernández-Lodeiro, A.; Pérez-Juste, J.; Pastoriza-Santos, I.; LaGrow, A. P.; Schraidt, O.; Luis Capelo-Martínez, J.; Lodeiro, C. Polyallyl-amine Assisted Synthesis of 3D Branched AuNPs with Plasmon Tunability in the Vis-NIR Region as Refractive Index Sensitivity Probes. *J. Colloid Interface Sci.* **2022**, *611*, 695−705.

(23) Fu, G.; Han, W.; Yao, L.; Lin, J.; Wei, S.; Chen, Y.; Tang, Y.; Zhou, Y.; Lu, T.; Xia, X. One-Step Synthesis and Catalytic Properties of Porous Palladium Nanospheres. *J. Mater. Chem.* **2012**, *22* (34), 17604.

(24) Yin, S.; Wang, Z.; Liu, S.; Jiao, S.; Tian, W.; Xu, Y.; Li, X.; Wang, L.; Wang, H. Flexible Synthesis of Au@Pd Core−Shell Mesoporous Nanoflowers for Efficient Methanol Oxidation. *Nanoscale* **2021**, *13* (5), 3208−3213.

(25) Rahaman, M.; Dutta, A.; Broekmann, P. Size-Dependent Activity of Palladium Nanoparticles: Efficient Conversion of CO_2 into Formate at Low Overpotentials. *ChemSusChem* **2017**, *10* (8), 1733−1741.

(26) Sylvestre, J.-P.; Kabashin, A. V.; Sacher, E.; Meunier, M.; Luong, J. H. T. Stabilization and Size Control of Gold Nanoparticles during Laser Ablation in Aqueous Cyclodextrins. *J. Am. Chem. Soc.* **2004**, *126* (23), 7176−7177.

(27) Lu, Y.; Zhang, J.; Ge, L.; Han, C.; Qiu, P.; Fang, S. Synthesis of Novel AuPd Nanoparticles Decorated One-Dimensional ZnO Nano-rod Arrays with Enhanced Photoelectrochemical Water Splitting Activity. *J. Colloid Interface Sci.* **2016**, *483*, 146−153.

(28) Wang, R.; Wu, Z.; Wang, G.; Qin, Z.; Chen, C.; Dong, M.; Zhu, H.; Fan, W.; Wang, J. Highly Active Au−Pd Nanoparticles Supported on Three-Dimensional Graphene−Carbon Nanotube Hybrid for Selective Oxidation of Methanol to Methyl Formate. *RSC Adv.* **2015**, *5* (56), 44835−44839.

(29) Dutta, S.; Ray, C.; Mallick, S.; Sarkar, S.; Roy, A.; Pal, T. Au@ Pd Core−Shell Nanoparticles-Decorated Reduced Graphene Oxide: A Highly Sensitive and Selective Platform for Electrochemical Detection of Hydrazine. *RSC Adv.* **2015**, *5* (64), 51690−51700.

(30) Yang, S.; Dong, J.; Yao, Z.; Shen, C.; Shi, X.; Tian, Y.; Lin, S.; Zhang, X. One-Pot Synthesis of Graphene-Supported Monodisperse Pd Nanoparticles as Catalyst for Formic Acid Electro-Oxidation. *Sci. Rep.* **2014**, *4* (1), 4501.

(31) Xiang, Y.; Wu, X.; Liu, D.; Jiang, X.; Chu, W.; Li, Z.; Ma, Y.; Zhou, W.; Xie, S. Formation of Rectangularly Shaped Pd/Au Bimetallic Nanorods: Evidence for Competing Growth of the Pd Shell between the {110} and {100} Side Facets of Au Nanorods. *Nano Lett.* **2006**, *6* (10), 2290−2294.

(32) Jiang, B.; Duan, D.; Gao, L.; Zhou, M.; Fan, K.; Tang, Y.; Xi, J.; Bi, Y.; Tong, Z.; Gao, G. F.; et al. Standardized Assays for Determining the Catalytic Activity and Kinetics of Peroxidase-like Nanozymes. *Nat. Protoc.* **2018**, *13* (7), 1506−1520.